Counterflow Dielectrophoresis for Trypanosome Enrichment and Detection in Blood

Electronic Supporting Information

Authors : Anoop Menachery [1,†], Clemens Kremer [1,†], Pui E. Wong [2], Allan Carlsson [1], Steven L. Neale [1], Michael P. Barrett [2,*], Jonathan M. Cooper [1,*]

Affiliations:

[1]Department of Electronics and Electrical Engineering, The Bioelectronics Research Centre, College of Science and Engineering, Rankine Building, University of Glasgow, Glasgow, G12 8LT, Scotland, U.K .

[2]Wellcome Trust Centre for Molecular Parasitology, Institute of Infection, Immunity and Inflammation, College of Medical, Veterinary and Life Sciences Sir Graeme Davies Building, 120 University Place, G12 8TA, Scotland, U.K .

[†] Both authors have contributed equally to this study

[*] To whom all correspondence should be addressed: Michael.Barrett@glasgow.ac.uk , Jon.Cooper@glasgow.ac.uk

Theory behind Cell Enrichment

In an active AC electrokinetic manipulation device, cells experience a combination of forces as they move through the fluid. Assuming negligible effects of gravity and substrate adhesion, the equation of motion is given by

$$m\frac{d\boldsymbol{v}}{dt} = \boldsymbol{F}_{DEP} + \boldsymbol{F}_{int} + f(\boldsymbol{u} - \boldsymbol{v}) \qquad [\mathbf{1}]$$

where $\boldsymbol{F}_{DEP}$ is the DEP force acting on the particle, $\boldsymbol{F}_{int}$ is the intrinsic force exerted by a motile cell, m is the mass of the particle, f is the friction factor and $\boldsymbol{v}$ is the velocity of the particle. Fluid movement in AC electrokinetic experiments, assigned a velocity $\boldsymbol{u}$, primarily results from electrosmotic flow, electrothermal flow or an external fluid pump. The drag force $f(\boldsymbol{u} - \boldsymbol{v})$ experienced by the particle, is dependent on the size and shape of the particle and the viscosity of the fluid. Trypanosomes exhibit an inherent motility, but do not exhibit directionality. Consequently, even though the intrinsic force, $\mathbf{F}_{\text{int}}$, cannot be neglected during entrapment at the electrode edges, during the time course of the experiment the net displacement can be assumed to be insignificant. Assuming negligible effects of gravity and substrate adhesion, the cells undergoing motion in a fluid under the influence of an external force will have an average velocity that is proportional to the induced DEP force.

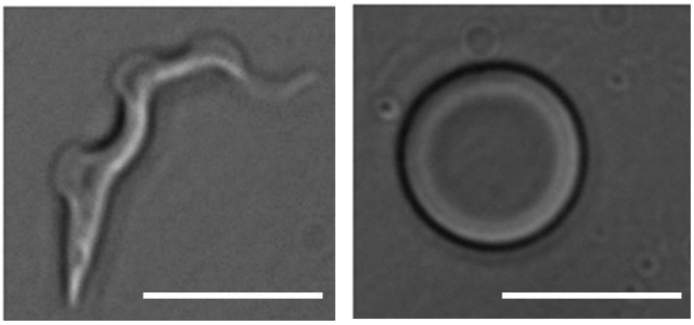

Fig. S1. An image of a trypanosome and RBC, the scale bar is 8µm.

Characterisation of Cross-Over Frequencies

Experimental characterisation of >30 cells in working solutions of different conductivities varying from 16 mS/m to 60 mS/m are shown in Fig. S2. For trypanosomes, the frequencies ranged from 20 kHz to 150 kHz. For Mouse RBCs crossover frequencies ranged from 100 kHz to 380 kHz, whereas for human RBCs, values were found to vary from 60 kHz to 260 kHz. For a solution conductivity of 30 mS/m, the optimal enrichment frequency was determined to be ~140 kHz for trypanosomes among mouse RBCs. The larger crossover frequencies for mouse RBCs can be attributed to a smaller mean diameter of 6 µm compared to 8 µm for human RBCs.

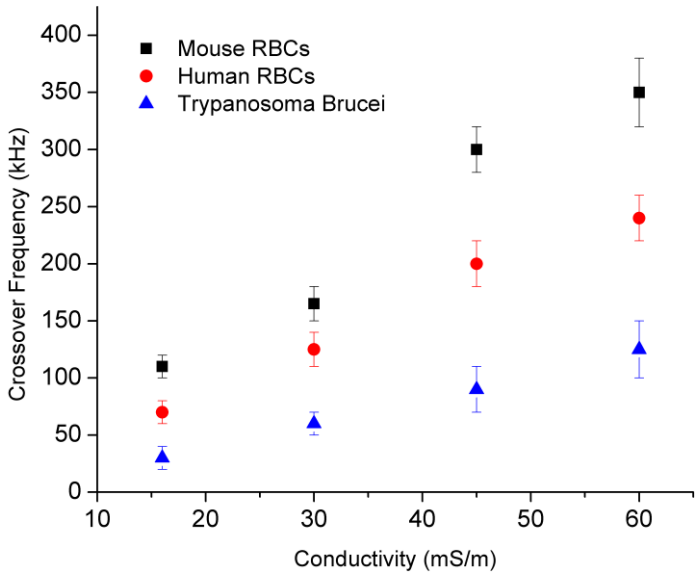

Fig. S2. Correlation between solution conductivity (16, 30, 45 and 60 mS/m) and capture frequency of mouse RBCs, human RBCs and trypanosomes. >30 cells were evaluated per data point, error is standard deviation.

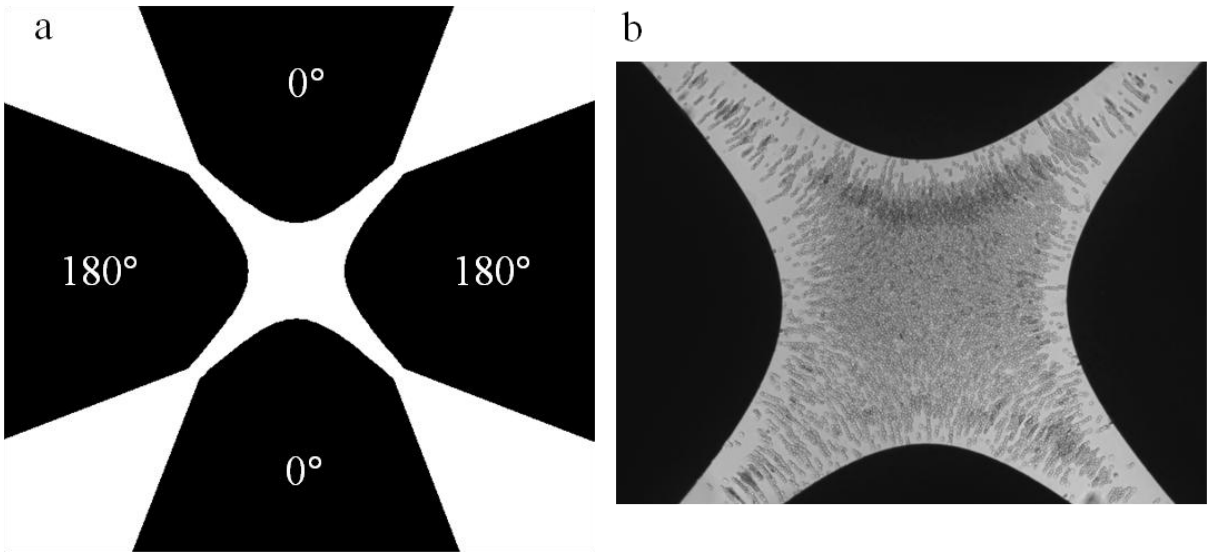

Fig. S3. Quadrupole electrodes used for characterisation of cross-over frequencies. (a) Schematic of the quadrupole electrode array, with an interelectrode separation of 400 μm (from tip to tip). (b) Human red blood cells undergoing negative DEP at 40 kHz, 30mS/m conductivity.

Simulations

To understand the influence of the travelling electric field, simulations were performed using *COMSOL Multiphysics*, a finite element analysis simulation software, using a 2D geometric model of adjacent electrodes within Fig. 1 (main text), with a 30 μm spacing. For TWDEP, four signals with phase shifts of 90° were used to generate a traveling electric field with a spatially dependent phase. The magnitude and phase of the applied electric potential was written as $\boldsymbol{V = V_r + jV_i}$, where $\boldsymbol{V_r}$ is the real part of the electric potential and $\boldsymbol{V_i}$ is the imaginary part of the electric potential.

The values for the real and imaginary part of the electric potential were assigned a peak amplitude of 1V, corresponding to the experimental conditions. After imposing the necessary boundary condition restrictions (*2*), shown in Fig. S4, the potential distribution was determined by solving Laplace's equation for the real and imaginary parts of the potential phasor. The electric field $\boldsymbol{E}$ is calculated using $\boldsymbol{E = -\nabla V}$, and this is used to estimate the DEP force components.

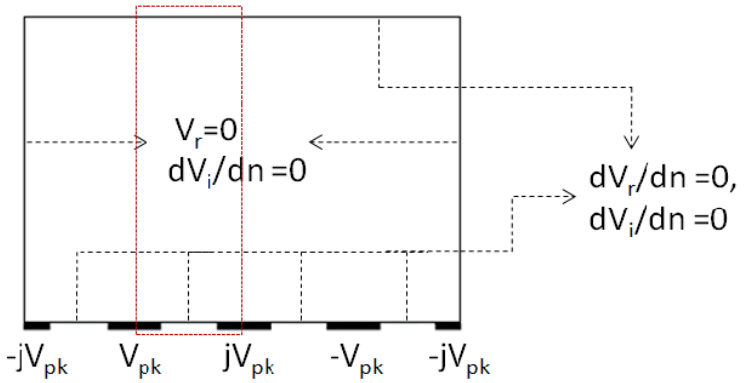

Fig. S4. A schematic drawing of the 4-phase travelling wave electrode array showing the boundary conditions for solving Laplace's equation. The dotted rectangle represents a section of the simulation shown in Fig. 2 (main text) & Fig. S5.

In Fig. S5 (a), the $\boldsymbol{\nabla E^2}$ vector direction for positive DEP conditions ($\boldsymbol{Re(CM)} > 0$) is vertically downwards onto the electrode edges. For negative DEP conditions ($\boldsymbol{Re(CM)} < 0$), the vector arrows will be directed upwards, reverse orientation to those shown in Fig. S5 (a), resulting in the levitation of cells above the electrode plane. The ∇E^2 factor is maximum at the edge of the electrodes with a value greater than 10^{16} V^2/m^3. The DEP force extends above the electrode, but with decreasing strength, i.e. at 20 μm above the electrode surface, the factor ∇E^2, has decreased by two orders of magnitude.

Fig. S5 (b) shows the direction and magnitude of $E_{xo}^2 \nabla \varphi_x + E_{yo}^2 \nabla \varphi_y + E_{zo}^2 \nabla \varphi_z$ vectors above a four-phase electrode array. It can be observed that for heights > 10 μm above the electrode plane, the vectors point to the right, but for heights < 10 μm, these vectors point in the opposite direction.

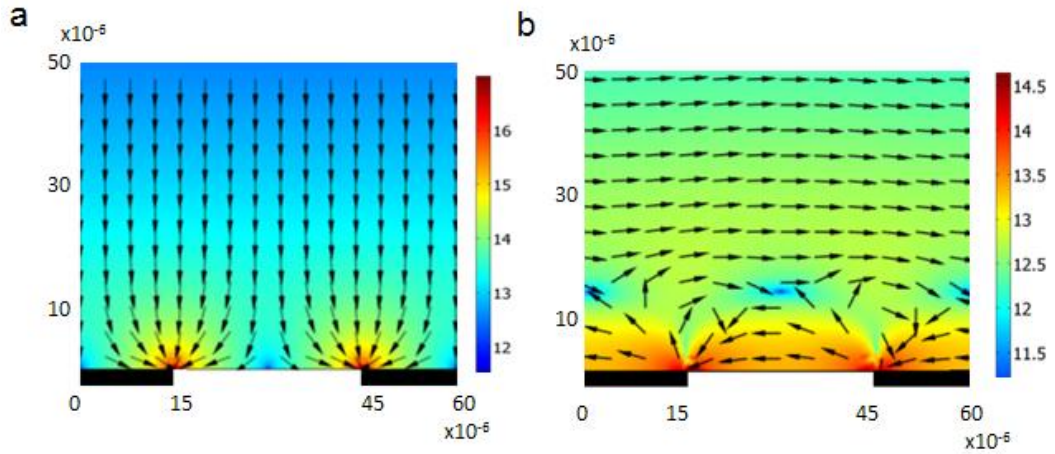

Fig. S5. A vertical section along the electrode plane showing the spatial variation of the DEP force components. The arrows represent the vector direction of the force components and the surface plot represents the magnitude of the force components (V^2/m^3, $\log_{10}$ scale). The x and y scale are in metres. (a) shows a spatial variation of ∇E^2 whilst (b) shows a spatial variation of $E_{xo}^2 \nabla \varphi_x + E_{yo}^2 \nabla \varphi_y + E_{zo}^2 \nabla \varphi_z$

The frequency-dependent polarisability response of trypanosomes and RBCs were also explored using a single shelled resistor-capacitor (RC) model of an ellipsoidal dielectric is implemented using a MATLAB (The Mathworks Inc.) environment. Similar dielectric models have been used to predict the polarization forces acting on biological cells using estimated dielectric parameters (*3*, *4*). The method used here to compute the effective polarisability of ellipsoids has been described by Gimsa et al (*1*). The model comprises of finite RC elements, represented by a complex conductivity σ^*, possessing equal cross-sectional area A and the length of each element l is given by the dimensions of the cytoplasm, membrane and the external medium. The length of the external medium element is set to a value which includes the effect of dipole field in the suspended medium.

The model consists of three impedance elements $Z_{i,a}^*$, $Z_{m,a}^*$ and $Z_{e,a}^*$, describing the interior of the cell, the cell membrane and the external medium respectively. An oblate ellipsoid model (a=b>c), where a, b and c are the semi-axes, is used for the RBCs and a prolate ellipsoidal model (a>b=c) is used for trypanosomes. The Clausius Mosotti factor CM_a of a cell oriented along its major axis is given by

$$CM_{a=}\frac{a_{infl}}{a_{infl-}a}\left(1-\frac{Z^*_{i,a}+Z^*_{m,a}}{Z^*_{i,a}+Z^*_{m,a}+Z^*_{e,a}}\frac{a_{infl}}{a}\right) \quad [2]$$

$$Z^* = \frac{1}{\sigma^*}\frac{l}{A}, \sigma^* = \sigma + j\omega\varepsilon_o\varepsilon_r \quad [3]$$

where $a_{infl}$is the influential axes that determines the maximum induced potential and ε_o and ε_r are the absolute and relative permittivity respectively.

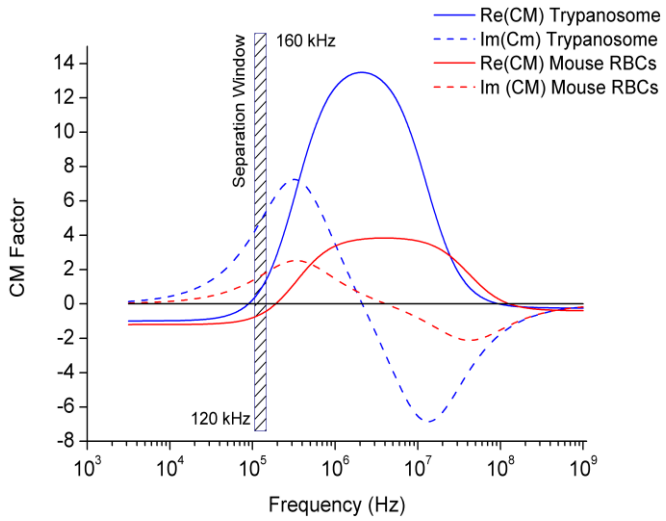

Fig. S6. Real and imaginary parts of the CM Factor for trypanosomes and mouse RBCs when their semi-major axis is oriented parallel to the electric field.

The dielectric parameters used in the model is detailed in Table S1.

Parameter	Mouse RBC value	Trypanasome value
Semi-major axis length (m)	3e-6	9e-6
Semi-minor axis length (m)	1.25e-6	1.2e-6
Membrane thickness (m)	7e-9	7e-9
Relative permittivities		
- Internal permittivity	60	60
-Membrane permittivity	12.5	19.8
-Medium permittivity	79	79
Conductivities (S/m)		
-Internal conductivity	0.8	0.8
-Membrane conductivity	1e-6	1e-6
-Medium Conductivity	30e-3	30e-3

Table S1. Dielectric parameter values used for RBCs and trypanosomes in a single shelled ellipsoidal RC model

Electrokinetic Fluid Flow

The travelling electric fields do not only induce cell movement, but can also result in a frequency dependent AC-electroosmotic and AC-electrothermal flow (*5-9*) in the fluid samples (the magnitudes of these effects varies

largely from what is negligible in comparison to the particle velocity, to a value which interferes greatly with the TWDEP driven particle motion).

AC electrosmosis is a result of the influence of a tangential electric field on the induced charge in an electrical double layer. AC electrosmosis is predominant in solutions with low ionic conductivities. When the fluid ionic strength increases, the Debye length of the double layer is reduced, resulting in a decreased AC electrosmosis velocity and an increase in the frequency at which AC electrosmosis velocity peaks. In contrast, AC electrothermal motion is a result of the changes in temperature through a conductive liquid, resulting in conductivity and permittivity gradients, which can give rise to fluid movement. The effect is greatest when the frequency equals the charge relaxation frequency of the media.

The velocity profile of AC electro-osmotic fluid movement is maximum near the electrode substrate and the frequency corresponding to the peak velocity can be estimated using $\approx \frac{\sigma \tau_D}{\varepsilon L}$, where L= 240 x 10^{-6} m and τ_D is the debye length. The debye length can be estimated using $\tau_D = \sqrt{\frac{\epsilon_o \epsilon_m \bar{R} T}{2F^2 c}}$, where $\bar{R}$ is the gas constant , T is the absolute temperature , F is the Faraday constant and c is the concentration of ions. For an experimental conductivity of 30 mS/m, the Debye length is calculated to be 6.3 nm. The peak velocity can be estimated to occur at ~ 1.1 kHz, which is lower than the frequency value of 140 kHz used in the experiments reported here, but limited AC electro-osmotic pumping in the direction of the travelling electric field can be expected.

Fluid movement due to an AC electrothermal effect can be neglected, since it is strongest when the applied frequency matches the charge relaxation time of the medium, when $f = \frac{\sigma}{2\pi \epsilon_o \epsilon_m}$,which is calculated to be 6.8 MHz, which is significantly higher than a value of 140 kHz used in the experiments reported here. Conductivities of 30 mS/m with a voltage of 1V peak are insufficient to cause an appreciable temperature gradient to induce significant fluid flow.

Frequency Dependence of Trypanosome Movement.

The frequency dependence on the movement of trypanosomes was investigated in a range from 100 kHz to 160 KHz, shown in Fig. S7 (b). An increase in enrichment numbers is observed for frequencies ranging from 100 kHz to 140 KHz, but at a frequency of 160 KHz, the enrichment numbers begin to fall due to increased trapping of RBCs at the electrode edge, thereby impeding the trypanosome movement into the centre of the spiral. The gradual increase in velocity with increase in frequency can be attributed to an increase in the real and imaginary parts of the CM factor which helps to keep the trypanosome closer to the electrode plane and provides stronger translational forces into the centre of the spiral.

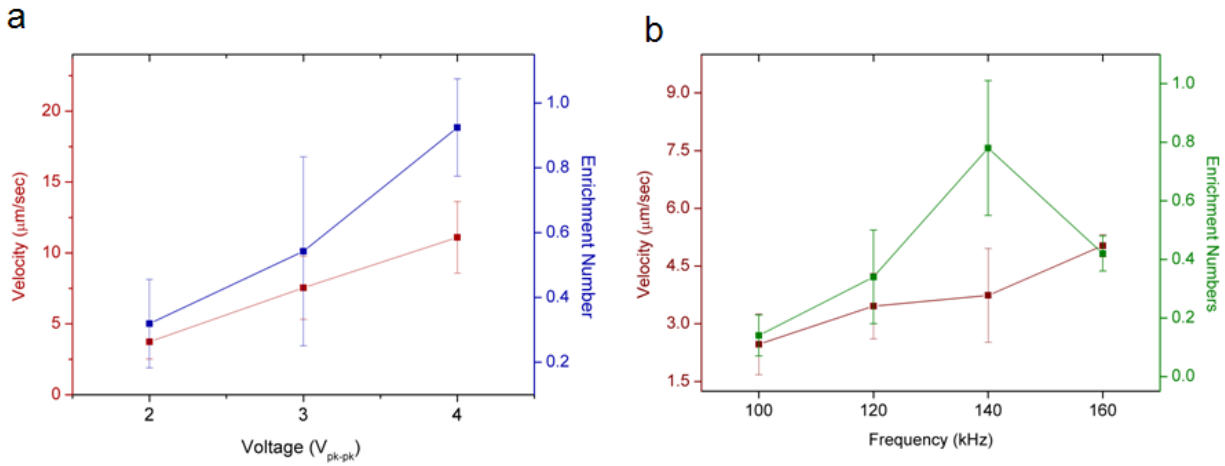

Fig S7. Correlation between the AC voltage parameters of the travelling electric field and the trypanosome velocity and enrichment numbers (a) voltage dependence (b) frequency dependence. >7 experiments were evaluated per data point, error is standard deviation.

Sensitivity

The sensitivity of the system as defined here is the number of parasites detected in the centre of the spiral after the experiment, compared to the number of parasites that were contained in the sampling volume (see below) during the experiment. In contrast, the limit of detection is the minimum number of parasites that have to be present in a sample for the test to give a positive result.

The sampling volume is the volume of liquid above the electrode array. Given a total diameter of 2.9 mm of the spiral array and a height of 150um, the sampling volume is approximately 1 µl of liquid (a cylinder with a radius of 1.45mm and a height of 0.15mm). Assuming a sensitivity of 100% (that is every single parasite on top of the spiral is concentrated into the centre) this already gives a limit of detection of $1x10^3$ parasites per ml of whole blood. However in order to reduce the conductivity of the medium to the required value the sample is diluted 1:40 with buffer raising the limit of detection to $4x10^4$ parasites/ml.

Under real experimental conditions the sensitivity is never 100% as some parasites are pushed out of the spiral together with red blood cells undergoing TWDEP. Experimental values were determined for different dilutions of paraites/ml of blood. For optimal enrichment conditions (140 kHz, 2 Vpp) and a low level of parasitemia (~10^5 trypanosomes/ml of whole blood prior to dilution) sensitivity was about 50%.

Consequently we assume that 3 parasites are necessary to be present in the sampling volume to concentrate at least one into the centre of the array. This gives the value of $1.2x10^5$ parasites/ml presented here in the paper. It can be seen from these calculations that the main limiting factor is not the sensitivity of the device but rather the dilution of the sample and the small sampling volume. Both can be addressed by increasing the sampling volume. Increasing the diameter of the spiral to about 1cm (without changing the height of the chamber) will increase the sampling volume to approximately 12µl. Provided the sensitivity of the device is not decreased (and we see no reason why this would be the case) this will lower the limit of detection to ~$1x10^4$ trypanosomes/ml.

10 such spirals in parallel would give a limit of detection of ~1x10^3 and this value could be decreased even further with additional up-scaling. It should be noted that the same effect can be achieved with 120 smaller spirals in parallel, but this kind of configuration would complicate the loading of the sample as it would require 120 different wells to be filled (instead of 10).

Another way the limit of detection could be lowered would be to increase the sensitivity by including an additional dielectrophoretic step in which the cells are just separated in height before the TWDEP force is applied (opposing two-phase configuration for traditional DEP). This technique, which will be explored in future work, will not cause any cells to be pushed out of the spiral while the parasites become trapped at the bottom of the chamber before the TWDEP force is applied to concentrate them.

References

1. J. Gimsa, *A comprehensive approach to electro-orientation, electrodeformation, dielectrophoresis, and electrorotation of ellipsoidal particles and biological cells*. Bioelectrochemistry **54**, 23-31 (2001).
2. N. G. Green, A. Ramos, H. Morgan, *Numerical solution of the dielectrophoretic and travelling wave forces for interdigitated electrode arrays using the finite element method*. Journal of Electrostatics **56**, 235-254 (2002).
3. K. Asami, Y. Takahashi, S. Takashima, *Dielectric properties of mouse lymphocytes and erythrocytes*. Biochim Biophys Acta **1010**, 49-55 (1989).
4. R. Pethig, L. M. Jakubek, R. H. Sanger, E. Heart, E. D. Corson, P. J. Smith, *Electrokinetic measurements of membrane capacitance and conductance for pancreatic beta-cells*. IEE Proc Nanobiotechnol **152**, 189-193 (2005).
5. B. P. Cahill, L. J. Heyderman, J. Gobrecht, A. Stemmer, *Electro-osmotic streaming on application of traveling-wave electric fields*. Phys Rev E Stat Nonlin Soft Matter Phys **70**, 036305 (2004).
6. I. R. Perch-Nielsen, N. G. Green, A. Wolff, *Numerical simulation of travelling wave induced electrothermal fluid flow*. J. Phys. D: Appl. Phys. **37**, 2323-2330 (2004).
7. H. C. Yeh, R. J. Yang, W. J. Luo, *Analysis of traveling-wave electro-osmotic pumping with double-sided electrode arrays*. Phys Rev E Stat Nonlin Soft Matter Phys **83**, 056326 (2011).
8. G. Giraud, R. Pethig, H. Schulze, G. Henihan, J. G. Terry, A. Menachery, I. Ciani, D. Corrigan, C. J. Campbell, A. R. Mount, P. Ghazal, A. J. Walton, J. Crain, T. T. Bachmann, *Dielectrophoretic manipulation of ribosomal RNA*. Biomicrofluidics **5**, 24116 (2011).
9. A. Ramos, H. Morgan, N. G. Green, A. González, A. Castellanos, *Pumping of liquids with traveling-wave electroosmosis*. J. Appl. Phys. 97 **97**, 084906-084901 - 084906-084908 (2005).